Alternative voltammetry on self-assembled monolayers: An original approach to estimate the electrochemical electron-transfer rate constants when electroactive adsorbed species interact

Olivier Alévêque, Eric Levillain, Yohann Morille

Contents lists available at ScienceDirect

Journal of Electroanalytical Chemistry

journal homepage: www.elsevier.com

Alternative voltammetry on self-assembled monolayers: An original approach to estimate the electrochemical electron-transfer rate constants when electroactive adsorbed species interact

Olivier Alévêque *, Eric Levillain , Yohann Morille

Université d'Angers, CNRS UMR 6200, Laboratoire MOLTECH-Anjou, SFR MATRIX, 2 boulevard Lavoisier, 49045 Angers Cedex, France

ARTICLE INFO

Keywords:
Alternative voltammetry
Lateral interactions
Electroactive self-assembled monolayers
Electrochemical simulations
Electrochemical fitting

ABSTRACT

This work presents original methodologies to estimate the electrochemical electron-transfer rate constants (k_0) of immobilized electroactive species when strong intermolecular interactions occur in a redox-responsive material, for which the redox reaction is described by Butler–Volmer theory. Based on Laviron's equations and the initial Creager and Wooster's work, these methodologies encompass the general lateral interaction model and have been experimentally tested to estimate k_0 in order to provide evidence of the relevance and reliability of our approach.

1. Introduction

Electrodes/Surfaces modified by a very thin film or a monolayer of molecules are proving to be a key point of research and development in a wide range of scientific fields. Since their discovery in 1983 [1], self-assembled monolayers (SAM) have always been the subject of extensive research and have become an ideal system for studying interfacial phenomena in detail. This is due to their simplicity of preparation, their relatively good stability and the possibility of modulating all parts of the grafted molecule such as the anchoring group, spacer and functional group in contact with the studied surfaces [2].

In this context, many models and theories have been developed [3,4] to extract quantitative information using electrochemical techniques as cyclic voltammetry [5], impedance spectroscopy [6], square-wave voltammetry, square-wave voltcoulometry [7], chronoamperometry [8,9], small-amplitude alternative voltammetry (AV) [10–12] and large-amplitude alternative voltammetry [13–15].

These last years, a great effort has been made to overcome some problems encountered and unsolved [16,17] with the first pioneered models in which molecules do not interact with each other. To obtain a more accurate prediction of experiments, a first approach, initiated by Laviron and based on Butler-Volmer kinetics formalism, consists in introducing global potential-independent intermolecular (lateral) interactions [18,19], which can be attractive or repulsive and depend on the redox state of immobilized molecules. This model, based on a Frumkin adsorption isotherm and the mean field theory, allows a perfect prediction of electrochemical experiments without explaining involved phenomena (Coulombic, Pi-Pi, Van der Waals interactions …). To extend this approach, alternatives have been developed including interactions with non-electroactive diluting molecules and supporting surface segregation [20–22].

Among available techniques that can support these models, cyclic voltammetry (CV) is today the most used technique to determine the values of intermolecular interactions and to estimate the electron-transfer rate constants (k_0) when k_0 is not to high ($<10\ s^{-1}$), via the Laviron's method [23]. Indeed, by CV, the Laviron's method requires the determination of the linear tangents at the boundary conditions ($v << k_0$ and $v >> k_0$) which remains very random for high scan rates (v). To overcome this limitation, Creager and Wooster developed, in 1998, an easy-to-use experimental method based on alternative voltametry experiments, involving to fit the ratio of the peak current to the background current relative to the logarithm of the frequency, in the case of non-interacting molecules [10]. The results obtained show that the AC Voltammetry makes it possible to obtain a much higher precision in the determination of rate constants than the CV can do, especially for high electron-transfer rate constants.

* Corresponding author.
Email address: olivier.aleveque@univ-angers.fr (O. Alévêque)

https://doi.org/10.1016/j.jelechem.2020.114414
Received 30 March 2020; Received in revised form 25 June 2020; Accepted 25 June 2020
Available online xxx

In this manuscript, we report original approaches to extend the Creager and Wooster's method to estimate the electrochemical electron-transfer rate constants (k_0) of immobilized redox probes when intermolecular interactions described by the general lateral interaction model are taken into account.

2. Alternative voltammetry dedicated to adsorbed systems

2.1. The general lateral interaction model

During the last few years, we proposed theoretical studies to update the lateral interaction model in order to include non-random distributions of electroactive species, interactions between redox and non-redox species and the possibility to used binary electrolyte mixture [21]. The generalized lateral interaction model (GLI model) enables current-voltage behaviours (CV, ACV) to be simulated in the case of a reversible n-electron redox reaction of adsorbed electroactive species, for which the redox reaction is described by Butler–Volmer theory:

$$O + ne^- \underset{kb}{\overset{kf}{\rightleftarrows}} R$$

For a better reading of the article, the GLI model is defined according to the main following hypotheses if we select only the case of interactions between redox species:

- The electroactive species are strongly adsorbed, so they are oxidized and reduced only at the adsorbed state,
- The electroactive species are distributed on substrate with a unimodal statistical distribution of electroactive neighbours, i.e. a single spatial distribution,
- A parameter $\phi(\theta)$, between 0 and 1, defined for a normalized surface coverage $\theta = \frac{\Gamma}{\Gamma_{max}}$ (Γ, the surface coverage in mol.cm^{-2}), quantifies the segregation level of the electroactive species. For a randomly distributed SAM, $\phi(\theta) = \theta$, and when a segregation exists on the surface, $1 > \phi(\theta) > \theta$,
- The sum of normalized surface coverage θ_O and θ_R of oxidized (O) and reduced (R) species is constant and equal to θ,
- The surface occupied by an oxidized molecule or a reduced molecule is the same,
- The electrochemical electron-transfer rate constant (k_0) is not dependent on the surface coverage,
- a_{OO}, a_{RR} and a_{OR} are the interaction constants between molecules of O, molecules of R and molecules of O and R, respectively. a_{ij} is positive for an attraction and negative for a repulsion.
- $G = (a_{OO} + a_{RR} - 2a_{OR})$ and $S = (a_{RR} - a_{OO})$ with $|G|$ and $|S| \leq 2$, are defined as "global interaction" parameters. When associated with $\phi(\theta)$, $G \cdot \phi(\theta)$ defines the shape of the voltammetric peak and modulates the FWHM and the peak intensity (i_p), whereas $S \cdot \phi(\theta)$ defines the position of the peak potential (E_p). In the case of high electron-transfer rate constants (k_0), under Nernstian conditions, these parameters are define as:

$$E_p(\theta) = E^{0\prime} + \frac{RT}{nF} S\,\phi(\theta)$$

$$I_p(\theta) = \frac{n^2F^2\nu A\Gamma_{max}}{2RT} \frac{\theta}{(2 - G\,\phi(\theta))}$$

$$FWHM(\theta) = \frac{2RT}{nF}\left[\ln\left(\frac{1+\sqrt{\frac{2-G\phi(\theta)}{4-G\phi(\theta)}}}{1-\sqrt{\frac{2-G\phi(\theta)}{4-G\phi(\theta)}}}\right) - G\phi(\theta)\sqrt{\frac{2-G\phi(\theta)}{4-G\phi(\theta)}}\right] \overset{|G\phi(\theta)|<1}{\approx} \frac{R}{nF}$$

and n, F, A, R, T E, $E^{0'}$ and v have their usual meanings.

2.2. Alternative voltammetry characteristics

Alternative Voltammetry used in this study involves the application of a sinusoidal voltage combined either with a steady DC voltage ($e(t) = E_{DC} + E_{AC}\sin(wt)$) or with voltage sweep at a scan rate v (V.s^{-1}) to a modified electrode surface ($e(t) = (E_i + \nu \cdot t) + E_{AC}\sin(wt)$). The later experiment is commonly named Alternative Cyclic Voltametry (ACV). The Fig. 1 shows two typical signals applied.

One of the most important aspect of an Alternative Voltammetry is the amplitude of the AC perturbation (E_{AC}), which needs to be small in comparison to the global change in voltage occurring during the experiment. Furthermore, the variation of the surface concentration of oxidized or reduced species needs to be small at each cycle in order to obtain a quasi-sinusoidal resulting current (Fig. 2), and allows the use of equivalent circuit and mathematical analysis [24]. In this case, it is possible to linearize the electrode kinetics, which initially have an exponential dependence on the applied voltage. Typically, a small ampli-

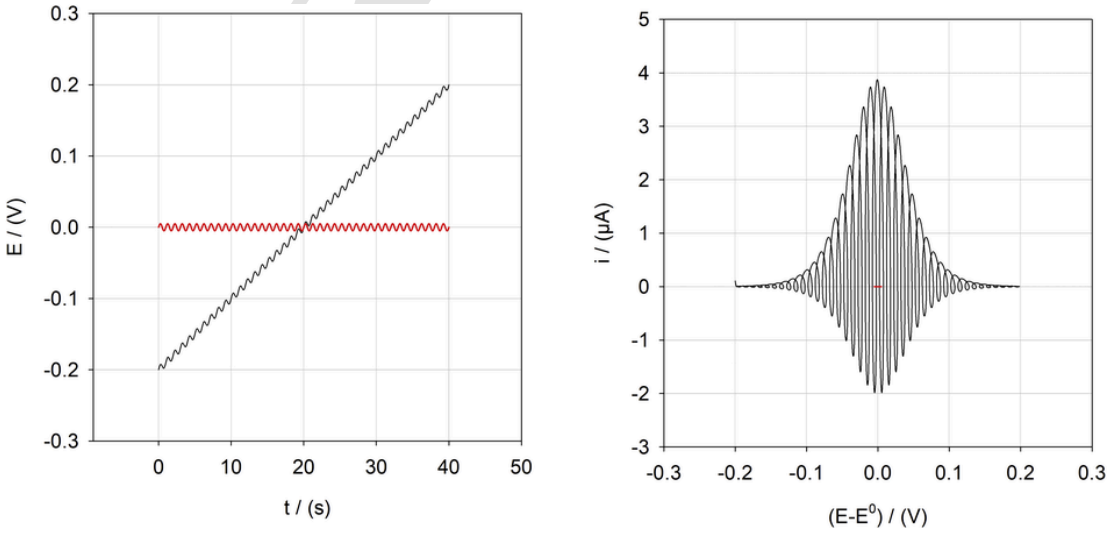

Fig. 1. (Left) Examples of alternative voltammetry applied potentials. (Red) Sinusoidal voltage combined with a steady DC voltage ($e(t) = E_{DC} + E_{AC}\sin(wt)$). (Dark) Sinusoidal voltage combined with a voltage sweep at a scan rate v (V.s^{-1}) ($e(t) = (E_i + \nu \cdot t) + E_{AC}\sin(wt)$). (Right) Resulting currents obtained with these two potential stimulations when applied to adsorbed systems. Note that the scan rate is deliberately high for readability reasons.

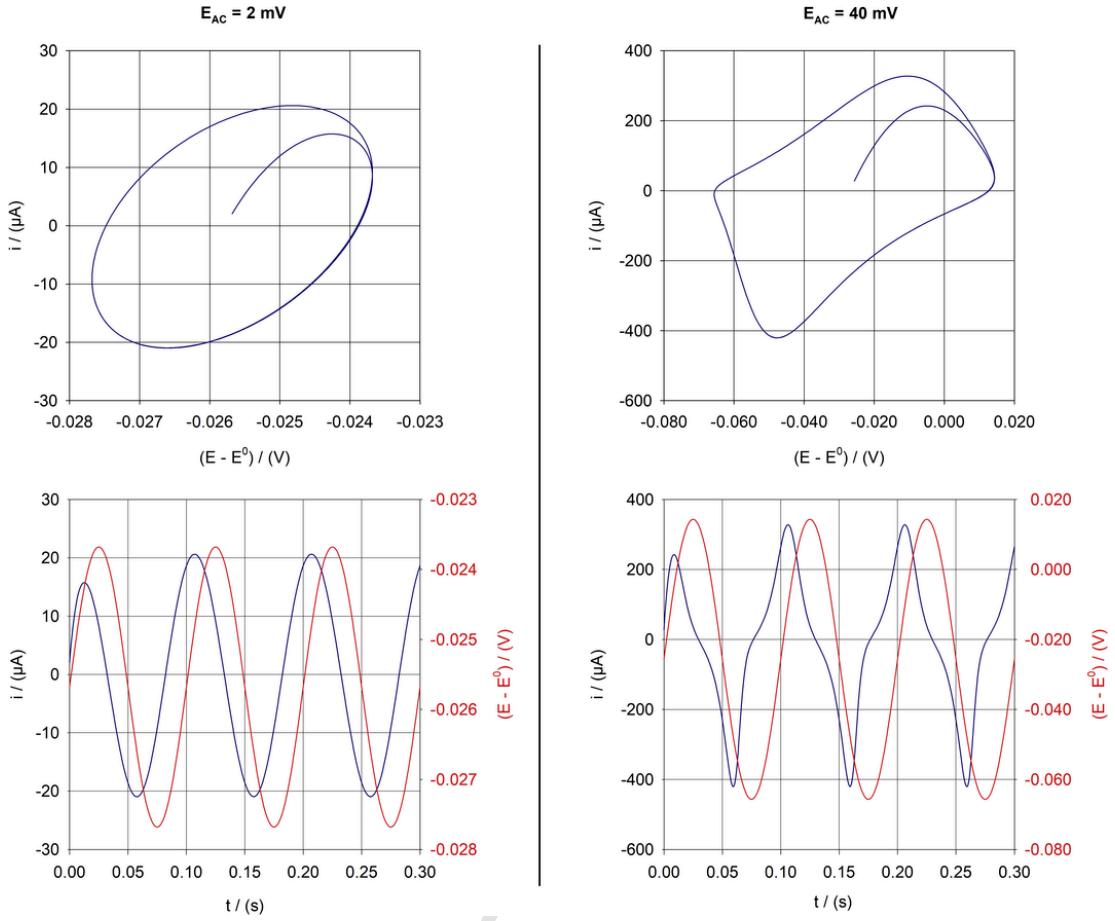

Fig. 2. ACV currents obtained at the cyclic voltammetry peak potential (E_{DC} = Ep), at 10 Hz and in the case of a_{oo} = 1, when the amplitude of the AC perturbation (E_{AC}) is 2 mV (left parts) or 40 mV (right parts).

tude of 10 mV or less is employed depending on interactions, especially in the case of attractive interactions that produce a rapid variation of the redox state of electroactive species close to apparent standard potential. Another important point concerns the value of the scan rate (v). It must be relatively low in order (1) to be in the conditions of electrochemical reversibility (Nernst conditions) and (2) to obtain an AC current much larger than the current obtained in the conditions of the cyclic voltammetry alone.

2.3. Generation of simulated voltammograms

All simulated cyclic voltammograms and alternative (cyclic) voltammograms were performed using MATLAB and/or SigmaPlot softwares and run on an conventional desktop computer (Intel Core i7-8650U CPU @ 1.90GHz). We used a numerical method approximating the continuous variation of the applied potential as a series of steps of size ΔE. If the increment ΔE is small enough, it is possible to assume that the rate constants k_b and k_f are constant during the entire increment.

This procedure is well detailed in previous papers [24] and adapted to our formalism. It can be written as:

$$i = nFA\Gamma_{\max}\frac{d\theta_O}{dt} = nFA\Gamma_{\max}\left(k_b\left(\theta-\theta_O\right)-k_f\theta_O\right)$$

$$\theta_O(i+1) = \left(\theta_O(i) - \frac{k_b(i+1)\,\theta}{k_b(i+1)+k_f(i+1)}\right)\exp\left(-\left(k_b(i+1)+k_f(i+1)\right)\Delta t\right) +$$

$$\Delta\theta_O = \theta_O(i+1) - \theta_O(i) = \left(\frac{k_b(i+1)\,\theta}{k_b(i+1)+k_f(i+1)} - \theta_O(i)\right)\left(1-\exp\left(-\left(k_b(i+1)\right.\right.\right.$$

$$\text{with}\begin{cases} \Delta t = \dfrac{\Delta E}{v} \\ \theta(j)\ \text{the value of}\ \theta_O\ \text{at step}\ j \\ k_b(i+1) = k_0\exp\left((1-\alpha)\dfrac{nF}{RT}\left(E(i+1)-E^{0\prime}\right)\right)\exp\left(-2\,a_{RR}\dfrac{\phi(\theta)}{\theta}\theta_R(\right. \\ k_f(i+1) = k_0\exp\left(-\alpha\dfrac{nF}{RT}\left(E(i+1)-E^{0\prime}\right)\right)\exp\left(-2\,a_{OO}\dfrac{\phi(\theta)}{\theta}\theta_O(i)\right. \\ E(i+1) = \left(E_i+vt\right)+E_{AC}\sin(wt) = \left(E_i+(i+1)\ \Delta t\,v\right)+E_{AC}\,s \end{cases}$$

3. Theoretical basis of alternative voltammetry dedicated to adsorbed systems

3.1. The formalism of Laviron

Three publications of Laviron have been devoted to the treatment of AC polarograms [11,12,25] in the case of strongly adsorbed electroactive species randomly distributed and presenting lateral interactions. Limited to the faradaic contributions (Fig. 3) of the adsorbed species (i.e. the charge transfer resistance (Rct) in series with the ad-

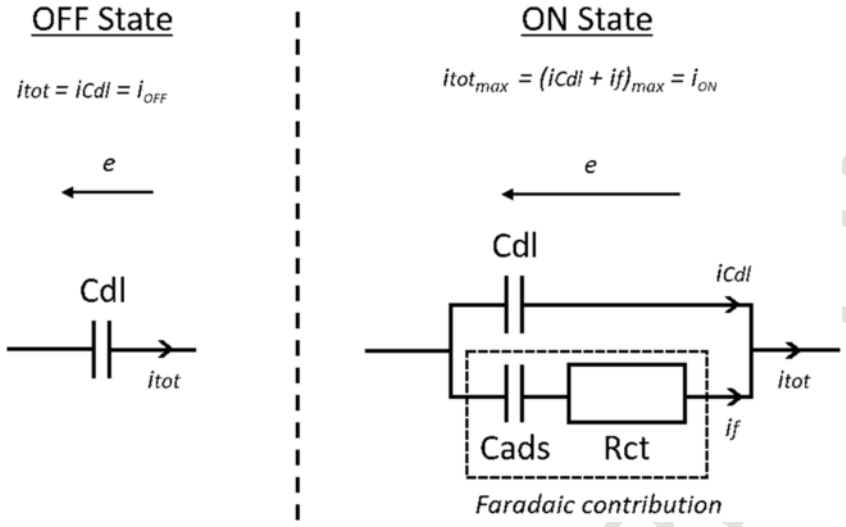

Fig. 3. Randles equivalent circuit with its two operating conditions used in this study. (left) an OFF state when no electrochemical reaction is produced, and (right) an ON state when the electrochemical system delivers its highest current.

sorbed capacitance (Cads)), the Laviron's approach allows to calculate the phase angle and magnitude of the current of AC polarograms.

The methodology used in these studies can be adapted to AC voltammetry, all principles and hypotheses staying the same.

Based on the Laviron's formalism, Rct and Cads can be expressed from the GLI model:

$$\begin{cases} Rct = \dfrac{RT}{n^2F^2A\Gamma_{max}}\dfrac{1}{k_0\chi} \\ \dfrac{1}{Cads} = \dfrac{RT}{n^2F^2A\Gamma_{max}}\dfrac{\xi}{\chi} \end{cases} \Rightarrow k_0\,\xi = \frac{1}{Rct\,Cads} \tag{3}$$

with

$$\begin{cases} \chi = (1-\alpha)\,\theta_R\eta^{1-\alpha}e^{-2a_{RR}\theta_R-2a_{OR}\theta_O} + \alpha\theta_O\eta^{-\alpha}e^{-2a_{OO}\theta_O-2a_{OR}} \\ \xi = \left(1+\left(a_{OR}-a_{RR}\right)\theta\right)\eta^{1-\alpha}e^{-2a_{RR}\theta_R-2a_{OR}\theta_O} + \left(1+\left(a_{OR}-a_{OO}\right)\theta\right)\eta^{-\alpha}e \end{cases}$$

Assuming thereafter the case of a charge transfer coefficient $\alpha = 0.5$ and a randomly distributed SAM ($\phi(\theta) = \theta$), these equations can be simplified:

$$\begin{cases} \chi = \sqrt{\theta_O\theta_R}e^{-\theta_O(a_{OO}+a_{OR})-\theta_R(a_{RR}+a_{OR})} = \sqrt{\theta_O\left(\theta-\theta_O\right)}e^{\theta_O S-\theta(a_{RR}+a_{OR})} \\ \xi = \chi\dfrac{\theta-2G\theta_O\theta_R}{\theta_O\theta_R} = \chi\dfrac{\theta-2G\theta_O(\theta-\theta_O)}{\theta_O(\theta-\theta_O)} \end{cases} \quad (\text{e}$$

At the equilibrium,

$$\begin{cases} \eta = e^{\frac{nF}{RT}(E-E^{0\prime})} = \dfrac{\theta_O}{\theta_R}e^{2\theta_O(a_{OR}-a_{OO})+2\theta_R(a_{RR}-a_{OR})} = \dfrac{\theta_O}{\theta-\theta_O}e^{-2G\theta_O+\theta(S+G)} \\ E^{0\prime} \textit{ is the surface standard potential} \\ E \text{ is the potential applied} \end{cases} \quad (\text{e}$$

Note that θ_O and θ_R are the values in the absence of alternative potential, at the equilibrium potential. To comply these conditions, (1) the experimental scan rate (v) must be lower than the electron-transfer rate constants (k_0) $\left(\frac{v}{k_0} \to 0\right)$, and (2) the AC perturbation (E_{AC}) needs to be small (see § 2.1). This places the system under Nernstian conditions around the equilibrium potential (i.e. at E_{DC} *or* $(E_i + v\cdot t)$).

It should be noted that Rct and Cads are not constant, but depend on the surface coverage of reduced and oxidized species, the interaction parameters and the α parameter.

3.2. The experimental approach of Creager and Wooster and its limitations

Based on Laviron's results, the Creager and Wooster's approach [10,26,27] uses the Randles equivalent circuit (Fig. 3), the most adapted for modelling a redox-active monolayer immobilized on electrode surface. Depending on the potential applied, the Randles equivalent circuit has two operating boundary conditions: an OFF state when no faradaic process occurs ($itot = iCdl = ioff = I_{OFF}\sin(wt + \varphi_{OFF})$) and an ON state when faradaic contribution is predominant and delivers a maximum alternative current ($itot_{max} = (iCdl + if)_{max} = ion = I_{ON}\sin(wt + \varphi_{ON})$).

By plotting the ratio of the magnitude of the peak current (I_{ON}) to the magnitude of the background current (I_{OFF}) of experimental AC voltammograms as a function of the logarithm of the frequency (f), a sigmoid curve is obtained, describing a cut-off phenomenon, which can be used to estimate k_0 by a fitting procedure. The resulting admittances of the circuit are:

$$\begin{cases} Y_{OFF} = w\,Cdl = 2\pi f Cdl \\ Y_{ON} = w\sqrt{\dfrac{Cads^2Cdl^2Rct^2w^2+Cads^2+2CadsCdl+Cdl^2}{Cads^2Rct^2w^2+1}} = 2\pi f Cdl\sqrt{\dfrac{\rho^2+\left(\frac{2\pi f}{k_0\xi}\right)}{1+\left(\frac{2\pi f}{k_0\xi}\right)}} \end{cases}$$

and $\rho = 1 + \dfrac{Cads}{Cdl}$

The Ion-to-Ioff ratio can be expressed as:

$$\frac{I_{ON}}{I_{OFF}} = \frac{Y_{ON}}{Y_{OFF}} = \sqrt{\frac{\rho^2+\left(\frac{2\pi f}{k_0\xi}\right)^2}{1+\left(\frac{2\pi f}{k_0\xi}\right)^2}} \tag{8}$$

ρ can be seen as the ratio $\frac{I_{ON}}{I_{OFF}}$ when $\frac{f}{k_0} \to 0$, as previously demonstrated.

In the particular case studied by the authors, without interaction between immobilized species and for $\alpha = 0.5$, the ACV peak potential (E_{ON}) at I_{ON} (i.e. the DC component of the potential applied), is located at $E^{0'}$ whatever the frequency (Fig. 4) and at this potential $\theta_{O\,ON} = \frac{\theta}{2}$, $\xi = 2$, $\chi = \frac{\theta}{2}$, $Rct = \frac{2RT}{n^2F^2A\Gamma_{max}k_0\theta}$, $Cads = \frac{n^2F^2A\Gamma_{max}\theta}{4RT}$ and $\rho = 1 + \frac{Cads}{Cdl}$

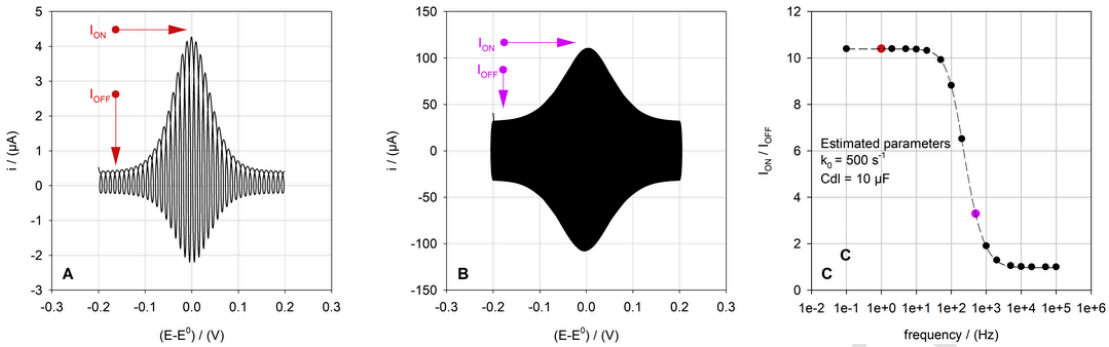

Fig. 4. ACV currents obtained at (A) f = 1Hz and (B) f = 500Hz ($\Gamma = 5.10^{-10}$ mol.cm^{-2}, $k_0 = 500$ s^{-1}, $E_{AC} = 5$ mV, v = 5 mv.s^{-1}, Cdl = 10 μF). (C) I_{ON}/I_{OFF} ratio obtained for each tested frequencies. The dotted line represents the best estimation obtained with fitted values: $k_0 = 500$ s^{-1} ($\sigma_{k0} = 0.001$ s^{-1}) and Cdl = 10 μF ($\sigma_{Cdl} = 0.001$ μF).

are constants. Consequently, $\frac{I_{ON}}{I_{OFF}}$ only depends on the ratio $\frac{f}{k_0}$, i.e. the one which can produce the well-known cut-off phenomenon (Fig. 4), and only two independent parameters are used to fit the sigmoid: k_0 and ρ.

As experienced by Laviron, the consideration of interactions between redox species induces drastic modifications on the expressions of χ and ξ and causes mathematical difficulties to solve equations due to the introduction of exponential terms. Indeed, without interaction, and according to previous equations, I_{ON} reaches its maximum at a particular value of $\theta_{O\,ON} = \frac{\theta}{2}$, which coincide with the inflection points of χ (maximum) and ξ (minimum) *vs.* θ_O. In the presence of interactions, the inflection points of χ (maximum) and ξ (minimum) are not positioned at the same value of θ_O, and according to Eqs. (7) and (8), I_{ON} needs to be maximized at each frequency with a specific couple (χ; ξ) associated to a specific $\theta_{O\,ON}$. Based on simulations of several current ratios, Fig. 5 shows a typical example of the variation of $\theta_{O\,ON}$ when frequency and interaction parameter a_{OO} vary. This frequency dependence of $\theta_{O\,ON}$ leads to a frequency dependence of associated parameters ξ, χ, *Rct*, *Cads* as well as the peak potential E_{ON}, according to a specific sigmoidal trend for each parameter.

Consequently, all these parameters, considered as constant without interaction, vary with frequency when interactions are present, which makes the Eq. (8) unusable for a fitting procedure, because $\frac{I_{ON}}{I_{OFF}}$ does not only depends on the ratio $\frac{f}{k_0}$ but also on $\theta_{O\,ON}(f)$.

Because no equation has been formulated so far to describe the variation of $\theta_{O\,ON}$ as a function of frequency, the Creager and Wooster's approach is used due to the lack of easy-to-use alternatives.

4. Results and discussion

4.1. Theoretical study

In order to study the $\frac{I_{ON}}{I_{OFF}}$ ratio with frequency when interactions are taking into account, the dependence of I_{ON} and $\theta_{O\,ON}$ with frequency must be clearly defined.

At ON state, the Randles equivalent circuit imposes, $i_{ON} = i_{Cdl} + i_f$, that can be rewritten as:

$$I_{ON}\sin\left(wt + \varphi_{ON}\right) = I_{Cdl}\sin\left(wt + \varphi_{Cdl}\right) + I_f\sin\left(wt + \varphi_f\right) \quad (9)$$

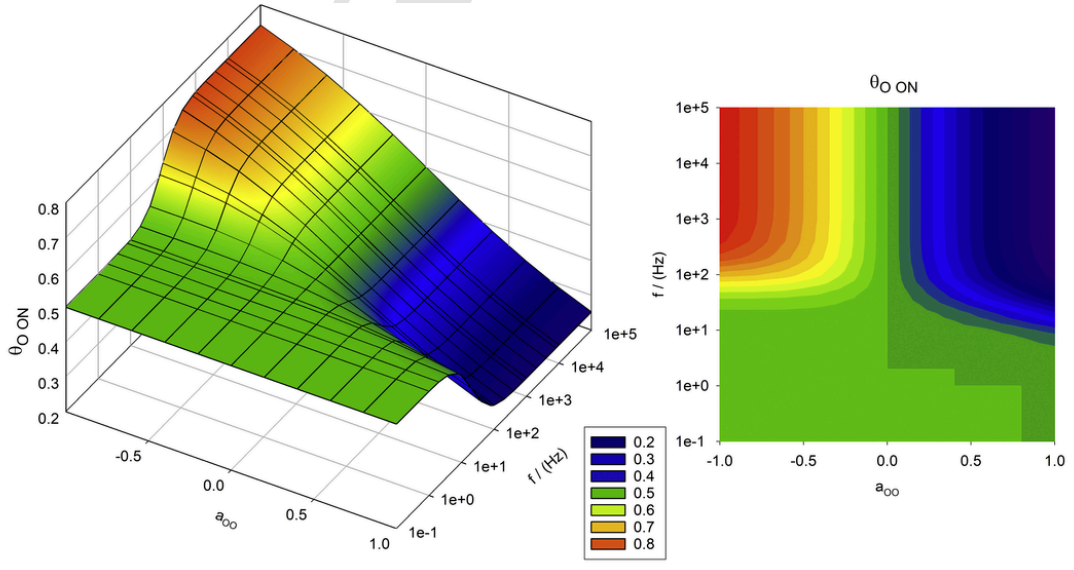

Fig. 5. Values of $\theta_{O\,ON}$ at different frequencies and interaction parameters a_{OO}, determined numerically with Eq. (8) (θ_O stepwise = 0.01, $k_0 = 100$ s^{-1}, Cdl = 10 μF and θ = 1).

with

$$\begin{cases} I_{Cdl} = w\,Cdl\,E_{AC} \\ \varphi_{Cdl} = \frac{\pi}{2} \end{cases} \quad and \quad \begin{cases} If = \frac{\frac{n^2F^2A\Gamma_{max}\theta}{RT}E_{AC}}{\sqrt{\left(\frac{1}{k_0\chi}\right)^2+\left(\frac{\xi}{w\chi}\right)^2}} \\ \varphi_f = \arctan\left(\frac{k_0\xi}{w}\right) \end{cases}$$

After simplifications (Appendix A), the magnitude of the current can be rewritten as:

$$I_{ON} = \sqrt{I_f^2 + 2I_fI_{Cdl}\sin(\varphi_f) + I_{Cdl}^2} = \sqrt{X_1 + I_{Cdl}^2} \tag{10}$$

With

$$X_1 = I_f^2 + 2I_fI_{Cdl}\sin(\varphi_f) = \frac{P^2}{\left(\frac{1}{k_0\chi}\right)^2+\left(\frac{\xi}{w\chi}\right)^2}\left(1+\frac{2\,Cdl}{P}\frac{\xi}{\chi}\right)E_{AC}^2$$

and

$$P = \frac{n^2F^2A\Gamma_{max}\theta}{RT}$$

In this expression, only theX_1 contribution is impacted by interaction parameters and θ_O (via χ and ξexpressions). Consequently, during an ACV experiment at a fixed frequency, $I_{ON}$is reached when the X_1 contribution is at its maximum, i.e. at a specified $\theta_{O\,ON}$ and so at a specified potential E_{ON}.

Derivation of X_1 with respect to θ_O must lead, after searching for zeros, to a particular value $\theta_{O\,ON}$ at which the current is maximum at a specified frequency. The non-linearity of the equations does not allow their full resolution and only solutions at the boundary conditions ($f\to 0$ or$f\to\infty$) can be calculated (Appendix B) as follow.

$$\begin{cases} \frac{f}{k_0} \to 0 \\ \theta_{O\,ONf\to 0} = \frac{\theta}{2} \end{cases}$$

$$\begin{cases} \frac{f}{k_0} \to \infty \\ \theta_{O\,ONf\to\infty} = \frac{(4\,Cdl\,G-P)(S\theta-1)-\sqrt{(4\,Cdl\,G-P)^2(S\theta-1)^2+2\cdot S\cdot\theta(4\cdot Cdl\cdot G-P)\cdot(4\cdot C}}{2S(4\,Cdl\,G-P)} \end{cases}$$

In addition when $\frac{f}{k_0}\to\infty$, some conditions are required on Cdl (Table 1, Appendix C), to reach a maximum between 0 and 1 ($0\le\theta_{O\,ON}\le 1$).

From Eq. (6), E_{ON} can be expressed as:

$$\begin{aligned} E_{ON} &= E^{0\prime} + \frac{RT}{nF}\left(\ln\left(\frac{\theta_{O\,ON}}{\theta-\theta_{O\,ON}}\right) - 2G\theta_{O\,ON} + \theta(S+G)\right) \\ E_{ON} - E_{ONf\to 0} &= \frac{RT}{nF}\left(\ln\left(\frac{\theta_{O\,ON}}{\theta-\theta_{O\,ON}}\right) + G\left(\theta - 2\cdot\theta_{O\,ON}\right)\right) \end{aligned} \tag{12}$$

with $E_{ONf\to 0} = E^{0\prime} + \frac{RT}{nF}\theta S = E_p$, i.e. the CV peak potential in reversible conditions.

Table 1
Conditions on Cdl to obtain $0 < \theta_{O\,ON} < 1$.

$G + \lvert S\rvert > 0$	$G + \lvert S\rvert < 0$
$0<Cdl<\frac{P}{4\left(G+\lvert S\rvert\right)}$	$0 < Cdl$

The same non-linearity excludes expressing $\theta_{O\,ON}$ as a function of E_{ON}.

In summary, no exact solution exists to describe $\theta_{O\,ON}$ at each frequency and especially around the $\frac{I_{ON}}{I_{OFF}}$ cut-off frequency, and at this stage, only $\theta_{O\,ON}$ at the boundary conditions ($f\to 0$ or$f\to\infty$) can be expressed.

4.2. Fitting procedures

To work around mathematical difficulties, we can nevertheless propose two different methods to determine the electrochemical electron-transfer rate constants using AV or ACV responses.

4.2.1. Fixed potential procedure

This first method is based on the Creager and Wooster's procedure without using the I_{ON} current because of its $\theta_{O\,ON}(f)$ dependence. If the magnitude of the total current (Itot) is recorded at a fixed value of θ_O, *i.e.* at a fixed value of potential E, the ratio of currents only depends on the frequency, and Eq. (8) can be adapted to:

$$\frac{\mathrm{Itot}_{\{E,\theta_O\}}}{\mathrm{I_{OFF}}} = \frac{\mathrm{Ytot}_{\{E,\theta_O\}}}{\mathrm{Y_{OFF}}} = \sqrt{\frac{\rho_{\{E,\theta_O\}}^2 + \left(\frac{2\pi f}{k_0\xi_{\{E,\theta_O\}}}\right)^2}{1+\left(\frac{2\pi f}{k_0\xi_{\{E,\theta_O\}}}\right)^2}} \text{ with parameters } \rho, \xi, \chi, \mathrm{Rct} \text{ and Cads constant} \tag{13}$$

Particularly, if the potential selected is the peak potential (E_p) of the initial cyclic voltammogram (reversible case), $E = E_p = E^{0\prime} + \frac{RT}{nF}\theta S$, $\theta_O = \frac{\theta}{2}$ and ρ, ξ, χ, *Rct* and *Cads* calculated with Eqs. (3), (4) and (5). Very easy to implement, this method can be used with the two types of Alternative Voltammetry (Alternative Voltammetry at a fixed potential or Alternative Cyclic Voltammetry). The key point is the measurement of $Itot_{\{E,\theta_O\}}$, the magnitude of the resulting sinusoidal current, which is less easy to determine than in the case of a peak. Indeed, during an ACV experiment, the current measured at the potential E is probably not the maximum current of the alternating cycle wherein E is included. Thus, either we use the maximum current closest to the potential E or the maximum current is estimated by drawing the upper envelope of the current. Fig. 6 highlights the principle of this procedure and shows the results of the fit and the estimation of k_0 using simulated alternative cyclic voltammograms for $a_{oo} = 1$. This fitting procedure makes it possible to determine the values of k_0 and Cdl with a good accuracy and precision in the case of interacting electroactive species.

4.2.2. Fitting procedure using the GLI function

Based on the General Lateral Interaction model, the GLI function has initially been developed to fit cyclic voltammetric peaks of self-assembled monolayers under Nernstian conditions for extracting characteristic parameters such as the peak current (i_p), the full width at half maximum (FWHM) and the peak potential (E_p).

$$i(E) = \frac{n^2F^2Av\Gamma_{max}\theta}{RT}\frac{\exp(X)}{(1+\exp(X))^2-2B\exp(X)}$$

$$\text{with} \begin{cases} X = \frac{nF}{RT}\left(E-E_p\right) + \frac{2B}{1+\exp\left(-\frac{nF}{RT}\left(E-E_p\right)\lambda\right)} - B \\ \lambda = 1/(1-\gamma\cdot B) \quad and \quad \gamma = 0.399 \\ B = G\phi(\theta) \text{ or } B = G\theta \text{ (random case)} \quad \text{and} \quad \lvert B\rvert < 2 \end{cases} \tag{14}$$

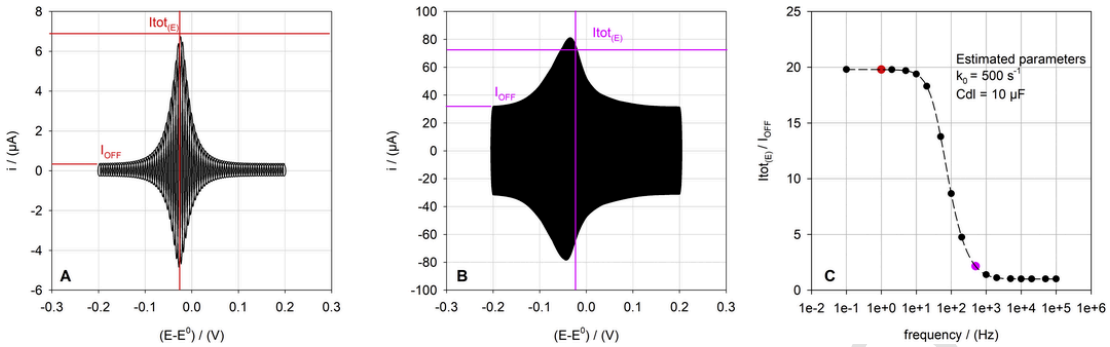

Fig. 6. ACV currents obtained at (A) f = 1Hz and (B) f = 500Hz ($\Gamma = 5.10^{-10}$ mol.cm^{-2} ($\theta = 1$), $k_0 = 500$ s^{-1}, $E_{AC} = 5$ mV, v = 5 mv.s^{-1}, Cdl = 10 μF, aoo = 1). (C) $Itot_{(E)}/I_{OFF}$ ratio obtained at the potential $E = E_p$ for each tested frequencies. The dotted line represents the best estimation obtained with fitted values: $k_0 = 500$ s^{-1} ($\sigma_{k0} = 0.001$ s^{-1}) and Cdl = 10 μF ($\sigma_{Cdl} = 0.001$ μF).

This equation is an approximation of the ratio $\frac{\theta_O}{\theta}$ to work around a problem of mathematical recursion.

$$\frac{\theta_O}{\theta} = \frac{1}{1+\exp\left(-\frac{nF}{RT}\left(E-E_p\right)\lambda\right)} \quad and \quad E-E_p = -\frac{RT}{nF\lambda}\ln\left(\frac{\theta-\theta_O}{\theta_O}\right) \tag{15}$$

The second approach proposed to determine the electrochemical electron-transfer rate constants using ACV responses consists in following simultaneously the ratio I_{ON}/I_{OFF} and the potential E_{ON} when frequency changes. Taking into account that $E_{ON\,f\to 0} = E_p$, $\theta_{O\,ON\,f\to 0} = \frac{\theta}{2}$, and using Eq. (14), E_{ON} and θ_{ON} can be defined as:

$$E_{ON} - E_{ON\,f\to 0} = -\frac{RT}{nF\lambda}\ln\left(\frac{\theta-\theta_{ON}}{\theta_{ON}}\right) \text{ and } \theta_{ON} = \frac{\theta}{1+\exp\left(-\frac{nF\lambda}{RT}\left(E_{ON}-E_{ON\,f\to 0}\right)\right)} \tag{16}$$

Ration I_{ON}/I_{OFF} is unchanged and is defined as:

$$\frac{I_{ON}}{I_{OFF}} = \sqrt{\frac{\rho^2+\left(\frac{2\pi f}{k_0\xi}\right)^2}{1+\left(\frac{2\pi f}{k_0\xi}\right)^2}}$$

with ξ, χ, *Rct*, *Cads and* ρ not constant but calculated with Eqs. (3), (4), (5) and with the estimation of $\theta_{O\,ON}$ (Eq. (15)) at each frequency. Finally, as desired, the ratio $\frac{I_{ON}}{I_{OFF}}$ only depends on the ratio $\frac{f}{k_0}$.

Fig. 7 shows the results of the fit and the estimation of k_0 using simulated alternative cyclic voltammograms. As in the previous case, this fitting procedure makes it possible to determine the values of k_0 and Cdl with a good accuracy and precision in the case of interacting electroactive species. It should be note that the intricate mathematical problem of the frequency dependence of E_{ON} and θ_{ON} induces that only the experimental points used can be recalculated after the fitting procedure, and thus the prediction of the ratio $\frac{I_{ON}}{I_{OFF}}$ at unmeasured frequencies is impossible.

All the results obtained with these two fitting procedures are listed in Table 2, and compared with those obtained with the Creager and

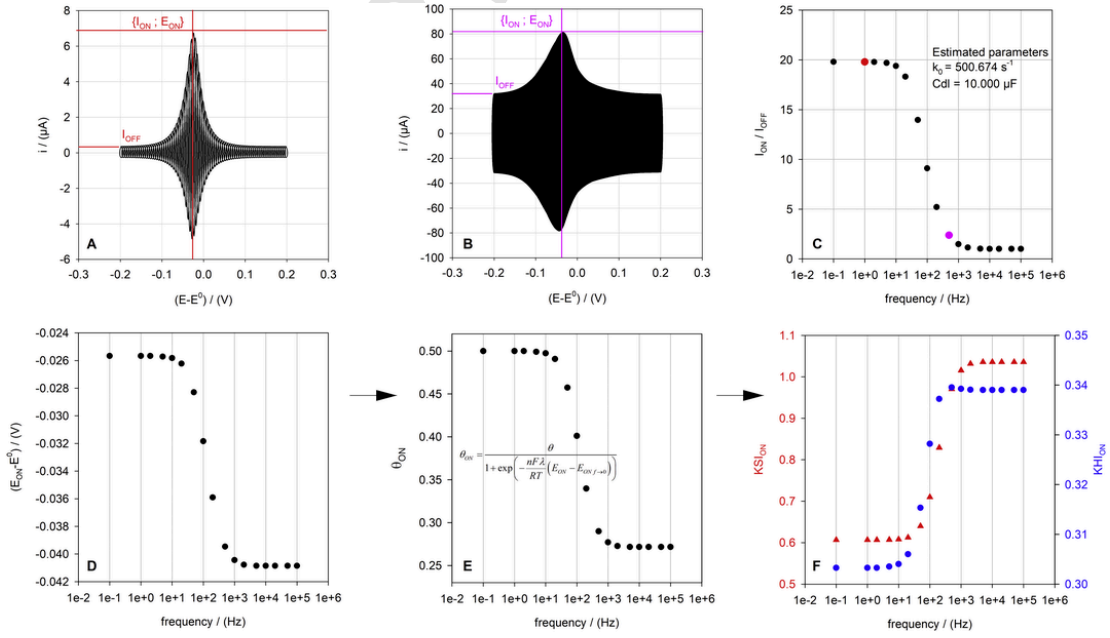

Fig. 7. ACV currents obtained at (A) f = 1Hz and (B) f = 500Hz ($\Gamma = 5.10^{-10}$ mol.cm^{-2} ($\theta = 1$), $k_0 = 500$ s^{-1}, $E_{AC} = 5$ mV, v = 5 mv.s^{-1}, Cdl = 10 μF, aoo = 1). (C) I_{ON}/I_{OFF} ratio obtained for each tested frequencies. (D) Potentials relative to each I_{ON}, which allow to calculate first (E) $\theta_{O\,ON}$, and secondly (F) χ_{ON} *and* ξ_{ON}. The best estimation obtained with fitted values is: $k_0 = 500.674$ s^{-1} ($\sigma_{k0} = 0.070$ s^{-1}) and Cdl = 10 μF ($\sigma_{Cdl} = 0.001$ μF).

Table 2
Results of the fitting processes ($\Gamma = 5.10^{-10}$ mol.cm^{-2} ($\theta = 1.00$), $k_0 = 500$ s^{-1}, $E_{AC} = 5$ mV, v = 5 mv.s^{-1}, Cdl = 10 μF, aoo = 1).

Simulated data	k_O (s^{-1})	σ_{k0} (s^{-1})	Cdl (μF)	σ_{CDL} (μF)
Creager and Wooster procedure	160.8	1.4	5.010	0.010
Fixed potential procedure	500.0000	0.0010	10.0000	0.0010
GLI function procedure	500.674	0.070	10.0000	0.0010

Wooster's procedure (without taking interactions into account). In this particular case of simulated voltammograms, the relative differences are 68% underestimated for k_0 and 50% underestimated for Cdl.

4.3. Fitting experimental ACV

4.3.1. Experimental setups

The relevance of our approach was experimentally tested by grafting a TEMPO derivative (C15-TEMPO) on Au substrate, known to provide very intense attractive interactions between its oxidized species ($a_{oo} = 1$) in methylene chloride. The synthesis, characterisations and preparation of C15-TEMPO-based SAM were described in Ref. [28].

Electrochemical experiments were carried out with a Biologic SP-300 potentiostat driven by the EC-Lab software including ohmic drop compensation. All electrochemical experiments (CV and ACV) were performed in a three-electrode cell controlled at a temperature of 293 K in a glove box containing dry, oxygen-free (< 1 ppm) argon. Working electrodes were a gold surface (A = 0.2 cm^2) modified with a C15-TEMPO SAM. Counter electrodes were platinum wires. Reference electrodes were Ag/$AgNO_3$ (0.01 M CH_3CN) in order to have a very fine determination of E_{ON}. Experiments were recorded in dry HPLC-grade methylene chloride with 0.1M tetrabutylammonium hexafluorophosphate (Bu_4NPF_6, electrochemical grade, Fluka) as supporting electrolyte.

The charge (Q) involved during a CV experiment is deduced by integration of the voltammetric signal, and the surface coverage of electroactive species is calculated as $\Gamma = Q/(nFA)$.

4.3.1.1. Cyclic voltammograms The first step aims at estimating interaction parameters of SAM. As mentioned previously, analysis of cyclic voltammograms under reversible conditions allows the extraction of the full width at half maximum (FWHM), peak potential (Ep) and peak intensity (ip) which depend on the interactions (Eq. (1)).

Figs. 8 and 9 show cyclic the voltammograms of the two SAMs covered with C15-TEMPO ($\theta = 0.64$ and $\theta = 0.18$). At these surface coverages, interaction parameters are calculated ($a_{OO} = 1 \rightarrow G = \frac{B}{\theta} = -S$) from the values of the FWHM, i_p, and E_p. E^0 is estimated at 0.553 V vs Ag/$AgNO_3$ reference electrode. In addition, Cdl can be roughly estimated at 1 μF by divided the capacitive current by the scan rate ($Cdl = i_{cap}/v$).

4.3.1.2. Alternative cyclic voltammograms The second step requires a set of ACV experiments on the same SAMs. Each ACV experiment was performed with a small amplitude voltage of 5mV (E_{AC}), a scan rate (v) of 5mV.s^{-1}, and an acquisition time adjusted to obtain 20 points per alternative cycle whatever the frequency used. Generally, three frequencies per decade were used between 1 HZ and 1000Hz (*i.e.* the maximum frequency of our instrument) to obtain the minimum number of points needed to perform the proposed adjustment procedures.

Figs. 8 and 9 show the experimental alternative cyclic voltammograms, at two frequencies (5 Hz and 200 Hz), of the two SAMs covered with C15-TEMPO.

4.3.2. Fitting procedures apply to experimental results

Figs. 8 and 9 show the $\frac{I_{ON}}{I_{OFF}}$ and $\frac{Itot_{\{E=Ep\}}}{I_{OFF}}$extracted from the same set of ACVs. The results of the fitting procedures applied to these data are listed in Table 3 and Table 4, and compared to the results obtained with the original Creager and Wooster's procedure (i.e. without interaction).

First of all, the two new procedures give fairly close results which validates the initial models and as previously observed, the original Creager and Wooster's procedure is clearly not suitable for determining k_0 and Cdl when interactions between redox species occur during the experiments, *i.e.* when $G\,\theta$ (or $G\,\phi(\theta)$) is not negligible. In the case of diluted monolayers, $G\,\theta$ tends to zero and the three procedures converge, as the theory predicts, towards quite similar results if the precision of the measurements is taken into account. The influence of the environment, the stability of the SAM and the poorer accuracy when the coverage is low may explain the slight differences observed.

Second, there is little differences between the two new procedures tested despite the fact that the GLI function is based on a model approximating the determination of θ_{ON}. This point is interesting because it opens up the possibility of choosing the adjustment procedure according to the technical capacities of the instrument used (AV or ACV). The weak point of the ACV method is the very high number of points required per experiment, which involves using a very efficient instrument.

The last important point is the good accuracy obtained in the determination of Cdl, as already observed with other alternative methods, compared to the determination with cyclic voltammetry [7,9].

5. Conclusion

Based on our previous studies on SAMs, Laviron's equations and the initial Creager and Wooster's approach, this work presents two general methods to estimate the electrochemical electron-transfer rate constants (k_0) of immobilized redox probes when the intermolecular interactions described by the general lateral interaction model are taken into account.

A thorough analysis of the AC voltammogram currents makes it possible to describe the cut-off phenomenon and to estimate k_0 by fitting procedures. The accuracy and precision of the results obtained, whether on simulated or experimental data, demonstrate the reliability of both procedures.

This work also shows that models or mathematical treatments [29] initially developed for cyclic voltammetry can be adapted and reused to exploit more complex techniques.

Acknowledgments

The authors thank Flavy Alévêque for her critical reading of the manuscript, and the plateau CARMA of the SFR MATRIX for the electrochemical characterisations.

Appendix A. Appendix

A.1. A1

$$I_{ON}\sin\left(wt+\varphi_{ON}\right) = I_{Cdl}\sin\left(wt+\varphi_{Cdl}\right) + I_f\sin\left(wt+\varphi_f\right)$$

According to trigonometric formula $\sin(a+b) = \sin(a)\cos(b) + \cos(a)\sin(b)$

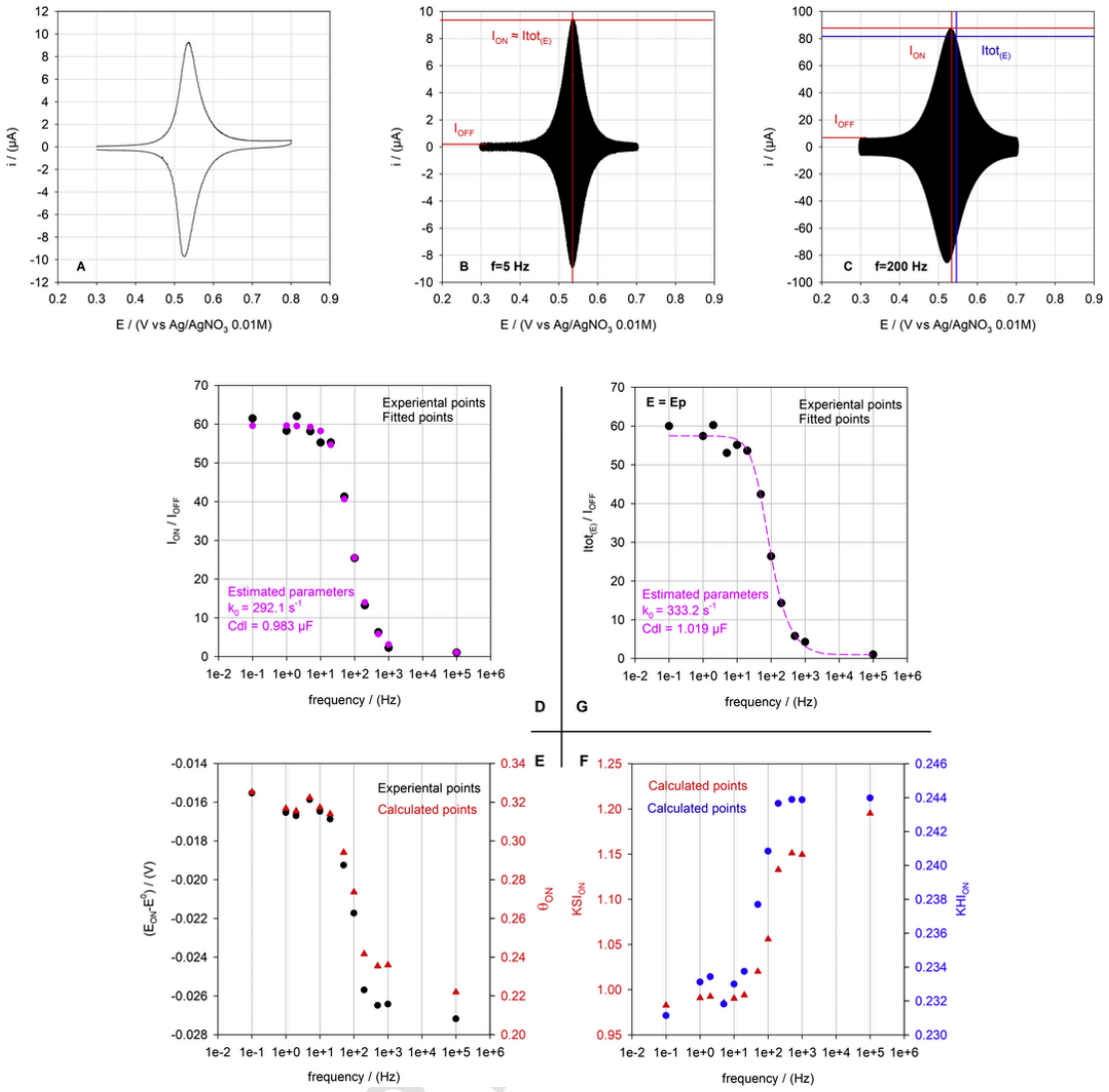

Fig. 8. Experimental CV and ACVs C15-T self-assembled monolayer ($\Gamma = 3.2.10^{-10}$ mol.cm^{-2} ($\theta = 0.64$), aoo = 1) in 0.1 M Bu_4NPF_6/CH_2Cl_2 at 293 K.Top) A) CV at v = 100 mV.s^{-1} (Ep = 0.536 mV vs $Ag/AgNO_3$), and ACVs (E_{AC} = 5 mV, v = 5 mv.s^{-1}) at B) 5 Hz and C) 200 Hz.Bottom) (D) I_{ON}/I_{OFF} ratio obtained for each tested frequencies. (E) Potentials relative to each I_{ON}, which allow to calculate first $\theta_{O\,ON}$, and secondly (F) χ_{ON} *and* ξ_{ON}. The best estimation obtained with fitted values is: $k_0 = 292.1$ s^{-1} ($\sigma_{k0} = 14.7$ s^{-1}) and Cdl = 0.983 µF ($\sigma_{Cdl} = 0.011$ µF). (G) $Itot_{(E)}/I_{OFF}$ ratio obtained at the potential $E = E_p$ for each tested frequencies. The dotted line represents the best estimation obtained with fitted values: $k_0 = 333.2$ s^{-1} ($\sigma_{k0} = 20.9$ s^{-1}) and Cdl = 1.019 µF ($\sigma_{Cdl} = 0.015$ µF).Note: to facilitate the calculation, the point at 10^5 Hz is a theoretical point.

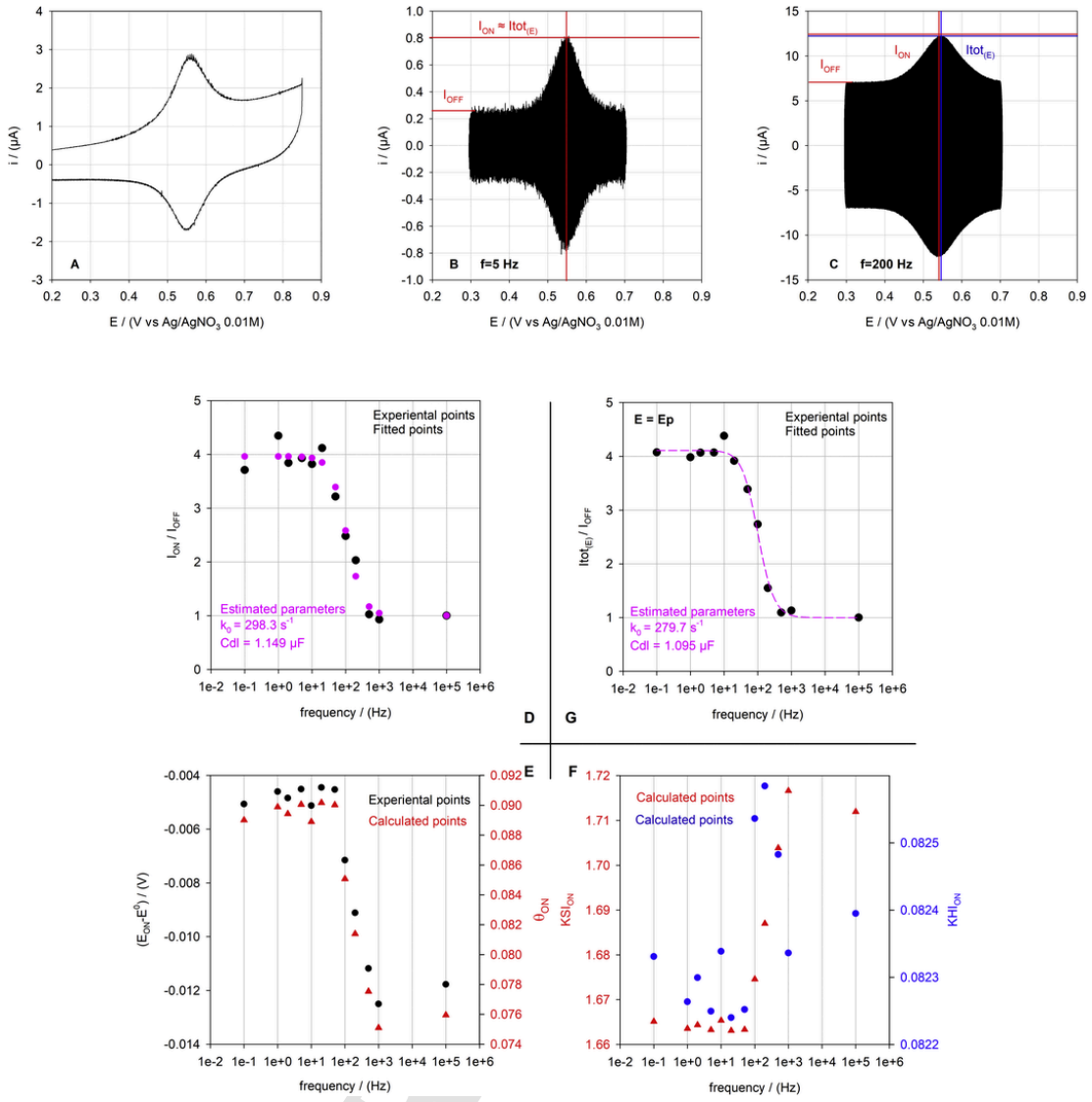

Fig. 9. Experimental CV and ACVs C15-T self-assembled monolayer ($\Gamma = 0.9.10^{-10}$ mol.cm^{-2} ($\theta = 0.18$), aoo = 1) in 0.1 M Bu_4NPF_6/CH_2Cl_2 at 293 K.Top) A) CV at v = 100 mV.s^{-1} (Ep = 0.552 mV vs $Ag/AgNO_3$), and ACVs (E_{AC} = 5 mV, v = 5 mv.s^{-1}) at B) 5 Hz and C) 200 Hz.Bottom) (D) I_{ON}/I_{OFF} ratio obtained for each tested frequencies. (E) Potentials relative to each I_{ON}, which allow to calculate first $\theta_{O\,ON}$, and secondly (F) χ_{ON} *and* ξ_{ON}. The best estimation obtained with fitted values is: $k_0 = 298.3$ s^{-1} ($\sigma_{k0} = 37.1$ s^{-1}) and Cdl = 1.149 µF ($\sigma_{Cdl} = 0.035$ µF). (G) $Itot_{(E)}/I_{OFF}$ ratio obtained at the potential $E = E_p$ for each tested frequencies. The dotted line represents the best estimation obtained with fitted values: $k_0 = 279.7$ s^{-1} ($\sigma_{k0} = 20.7$ s^{-1}) and Cdl = 1.095 µF ($\sigma_{Cdl} = 0.020$ µF).Note: to facilitate the calculation, the point at 10^5 Hz is a theoretical point.

Table 3
Results of the fitting processes ($\Gamma = 3.2.10^{-10}$ mol.cm^{-2} ($\theta = 0.64$), E_{AC} = 5 mV, v = 5 mv.s^{-1}, aoo = 1).

Experimental data	k_O (s^{-1})	σ_{k0} (s^{-1})	Cdl (µF)	σ_{CDL} (µF)
Creager and Wooster procedure	148.1	7.3	0.6692	0.0076
Fixed potential procedure	333.2	20.9	1.019	0.015
GLI function procedure	292.1	14.7	0.983	0.011

Table 4
Results of the fitting processes ($\Gamma = 0.9.10^{-10}$ mol.cm^{-2} ($\theta = 0.18$), E_{AC} = 5 mV, v = 5 mv.s^{-1}, aoo = 1)

Experimental data	k_O (s^{-1})	σ_{k0} (s^{-1})	Cdl (µF)	σ_{CDL} (µF)
Creager and Wooster procedure	248.9	31.0	1.046	0.032
Fixed potential procedure	279.7	20.7	1.095	0.020
GLI function procedure	298.3	37.1	1.149	0.035

$$I_{ON}\sin\left(wt+\varphi_{ON}\right)=I_{Cdl}\left(\sin(wt)\cos\left(\varphi_{Cdl}\right)+\cos(wt)\sin\left(\varphi_{Cdl}\right)\right)+I_f\left(s$$
$$I_{ON}\sin\left(wt+\varphi_{ON}\right)=\cos(wt)\left(I_{Cdl}\sin\left(\varphi_{Cdl}\right)+I_f\sin\left(\varphi_f\right)\right)+\sin(wt)$$
$$with\ A=\left(I_{Cdl}\sin\left(\varphi_{Cdl}\right)+I_f\sin\left(\varphi_f\right)\right)=I_{Cdl}+I_f\sin\left(\varphi_f\right)\ B=\left(I_{Cdl}\cos\left(\right.\right.$$
$$I_{ON}\sin\left(wt+\varphi_{ON}\right)=A\cos(wt)+B\sin(wt)=A\left(\cos(w\right.$$
$$I_{ON}\sin\left(wt+\varphi_{ON}\right)=A\left(\cos(wt)+\frac{\cos(\varphi)}{\sin(\varphi)}\sin(wt)\right)=\frac{A}{\sin(\varphi)}\left(\sin(\varphi)\cos(wt)+\right.$$

$$\tan(\varphi)=\frac{\sin(\varphi)}{\cos(\varphi)}=\frac{A}{B}\ \Rightarrow\ {I_{ON}}^2=\left(\frac{A}{\sin(\varphi)}\right)^2=A^2\left(1+\frac{1}{\tan(\varphi)^2}\right)=A^2+$$

$$I_{ON}=\sqrt{I_f^2+{I_{Cdl}}^2+2I_{Cdl}I_f\sin\left(\varphi_f\right)}=\sqrt{X_1+{I_{Cdl}}^2}\ with\ X_1=I_f^2+2I_{Cdl}I_f\,si$$

A.2. A2

$$\varphi_f=\arctan\left(\frac{k_0\xi}{w}\right)\qquad If=\frac{PE_{AC}}{\sqrt{\left(\frac{1}{ko\,\chi}\right)^2+\left(\frac{\xi}{w\chi}\right)^2}}\qquad II_{Cdl}=wCdlE_{AC}\ with$$
$$\sin\left(\varphi_f\right)=\sin\left(\arctan\left(\frac{k_0\xi}{w}\right)\right)=\frac{k_0\xi}{\sqrt{\left(k_0\xi\right)^2+(w)^2}}$$
$$X_1=I_f^2\left(1+2\frac{I_{Cdl}}{I_f}\sin\left(\varphi_f\right)\right)=\left(\frac{PE_{AC}}{\sqrt{\left(\frac{1}{k_0\chi}\right)^2+\left(\frac{\xi}{w\chi}\right)^2}}\right)^2\left(1+\frac{2wCdlE_{AC}-\right.$$
$$X_1=\frac{P^2}{\left(\frac{1}{ko\,\chi}\right)^2+\left(\frac{\xi}{w\chi}\right)^2}\left(1+\frac{2Cdl}{P}\frac{\xi}{\chi}\right){E_{AC}}^2$$

Appendix B. Appendix

B.1. Case

$$\lim_{\frac{f}{k_0}\to 0}X_1=\lim_{\frac{f}{k_0}\to 0}\frac{P^2}{\left(\frac{1}{k_0\chi}\right)^2+\left(\frac{\xi}{2\pi f\chi}\right)^2}\left(1+\frac{2Cdl}{P}\frac{\xi}{\chi}\right){E_{AC}}^2=P^2\left(\frac{2\pi f\chi}{\xi}\right)^2\left(1+\right.$$
$$A_1\ and\ A_2>0$$

This limit depends on the ratio $\frac{\chi}{\xi}=\frac{\theta_O(\theta-\theta_O)}{\theta-2G\theta_O(\theta-\theta_O)}$(see Eq. (5)), i.e. depends on θ_O.

This function is null at $\theta_O=0$ *and* $\theta_O=\theta$, is always positive for $\theta_O\in]\,0;\theta\,[$, and thus presents a maximum at $\theta_{O\,ON}$. The root of the θ_O-*derivative* of $\frac{\chi}{\xi}$ is equal to $\theta_{O\,ON}$, i.e. the particular value at which $\frac{\chi}{\xi}$ and X_1 are maximized.

$$\frac{d\left(\frac{\chi}{\xi}\right)}{d\theta_O}=\frac{-2\theta_O\theta+\theta^2}{\left(2G{\theta_O}^2-2G\theta_O\theta+\theta\right)^2};\ \frac{d\left(\frac{\chi}{\xi}\right)}{d\theta_O}=0$$
$$\Rightarrow\ \theta_{O\,ON}=\frac{\theta}{2}$$
$$\theta_{O\,ON}\in[0;\theta]$$

B.2. Case

$$\lim_{\frac{f}{k_0}\to\infty}X_1=\lim_{\frac{f}{k_0}\to\infty}\frac{P^2}{\left(\frac{1}{k_0\chi}\right)^2+\left(\frac{\xi}{2\pi f\chi}\right)^2}\left(1+\frac{2Cdl}{P}\frac{\xi}{\chi}\right){E_{AC}}^2=P^2\left(k_0\chi\right)^2\left(1+\frac{2}{}\right.$$
$$\lim_{\frac{f}{k_0}\to\infty}X_1=P^2{k_0}^2{\theta_O}\left(\theta-\theta_O\right)\left(\exp\left(S\theta_O+B\right)\right)^2\left(1+2Cdl\frac{\theta-2G\theta_O(\theta-\theta_O}{\theta_O(\theta-\theta_O)}\right.$$

This function is null at $\theta_O=0$ *and* $\theta_O=\theta$, is always positive for $\theta_O\in]\,0;\theta\,[$, and thus presents a maximum at $\theta_{O\,ON}$. The root of the θ_O-*derivative* of X_1 is equal to $\theta_{O\,ON}$, i.e. the particular value at which X_1 is maximized.

$$\frac{d(X_1)}{d\theta_O}=2Pk_0^2\left(\exp\left(S\theta_O-\theta\left(a_{RR}+a_{OR}\right)\right)\right)^2\left(S{\theta_O}^2(4CdlG-P)-(S\theta-1\right.$$
$$\frac{d(X_1)}{d\theta_O}=0\ \Rightarrow\ \left(S(4CdlG-P){\theta_O}^2-(S\theta-1)(4CdlG-P)\theta_O\right.$$
$$\theta_{O\,ON}=\frac{(4CdlG-P)(S\theta-1)-\sqrt{(4CdlG-P)^2(S\theta-1)^2+2S\theta(4C}}{2S(4CdlG-P)}$$
$$\theta_{O\,ON}\in[0;\theta]$$

Appendix C. Appendix

$$\frac{(4CdlG-P)(S\theta-1)-\sqrt{(4CdlG-P)^2(S\theta-1)^2+2\cdot S\cdot\theta(4\cdot Cdl\cdot G-P)\cdot(4\cdot Cdl\cdot(G-S)-P)}}{2S(4CdlG-P)}$$
$$=\frac{A-\sqrt{A^2+B}}{2S(4CdlG-P)}\quad with\quad\begin{cases}A=(4CdlG-P)(S\theta-1)\\B=2\cdot S\cdot\theta(4\cdot Cdl\cdot G-P)\cdot(4\cdot Cdl\cdot(G-S)-\end{cases}$$

C.1. Case $S<0$

$$S<0\ \Rightarrow\ 0<\theta_{O\,ONf=\infty}<\theta_{O\,ONf}<\theta_{O\,ONf=0}=\frac{\theta}{2}$$
$$\Rightarrow\ 0<\frac{A-\sqrt{A^2+B}}{2S(4CdlG-P)}<\frac{\theta}{2}$$

Hypothesis 1. $(4\,Cdl\,G-P)>0$

$$(4CdlG-P)>0$$
$$\Rightarrow\ \begin{cases}Cdl>\frac{P}{4G}\ for\ G>0\\Cdl<\frac{P}{4G}<0\ for\ G<0\ \ (impossible)\end{cases}$$

- $0<\frac{A-\sqrt{A^2+B}}{2S(4CdlG-P)}\ \Rightarrow\ A-\sqrt{A^2+B}<0$, which is always true (with some conditions on Cdl and G to obtain $\sqrt{A^2+B}>0$).
- $\frac{A-\sqrt{A^2+B}}{2S(4CdlG-P)}<\frac{\theta}{2}\ \Rightarrow\ A-\sqrt{A^2+B}>S\theta(4CdlG-P)$, that is impossible.
$$\Rightarrow\ -(4CdlG-P)-\sqrt{A^2+B}>0$$

These results invalidate this hypothesis.

Hypothesis 2. $(4\ Cdl\ G-P)<0$

$$(4\,Cdl\,G-P)\ <0$$
$$\Rightarrow \quad \begin{cases} 0<Cdl<\frac{P}{4G}\ for\ G>0 \\ Cdl>0>\frac{P}{4G}\ for\ G<0\ \ (always\ true) \end{cases}$$

$$0<\frac{A-\sqrt{A^2+B}}{2S(4\,Cdl\,G-P)} \quad \Rightarrow \quad A-\sqrt{A^2+B}>0$$

$$\Rightarrow \quad B=2\cdot S\cdot\theta\,(4\cdot Cdl\cdot G-P)\cdot(4\cdot Cdl\cdot(G-S)-P)<0$$
$$\Rightarrow \quad 4\cdot Cdl\cdot(G-S)-P<0 \quad \Rightarrow \quad \begin{cases} 0<Cdl<\frac{P}{4(G-S)}\ for\ (G-S)>0 \\ Cdl>0>\frac{P}{4(G-S)}\ for\ (G-S)<0\ \ (alwa \end{cases}$$

$$\frac{A-\sqrt{A^2+B}}{2S(4\,Cdl\,G-P)}<\frac{\theta}{2}$$
$$\Rightarrow \quad A-\sqrt{A^2+B}<S\theta\,(4\,Cdl\,G-P)$$
$$\Rightarrow \quad -(4\,Cdl\,G-P)-\sqrt{A^2+B}<0$$

$$\Rightarrow \quad (4\,Cdl\,G-P)^2<A^2+B$$
$$\Rightarrow \quad Cdl>0>\frac{P}{4}\frac{\theta}{G\theta-2} \quad (always\ true)$$

As a result, for $S<0$, required conditions are $\begin{cases} Cdl<\frac{P}{4(G-S)}\ for\ (G-S)>0 \\ Cdl>0\ for\ (G-S)<0 \end{cases}$.

C.2. Case S > 0

$$S>0 \quad \Rightarrow \quad S>0$$
$$\Rightarrow \theta>\theta_{OONf=\infty}>\theta_{OONf}>\theta_{OONf=0}$$
$$=\frac{\theta}{2}$$
$$\Rightarrow \quad \frac{\theta}{2}<\frac{A-\sqrt{A^2+B}}{2S(4\,Cdl\,G-P)}<\theta$$

Hypothesis 1. $(4\ Cdl\ G-P)>0$

$$(4\,Cdl\,G-P)\ >0$$
$$\Rightarrow \quad \begin{cases} Cdl>\frac{P}{4G}\ for\ G>0 \\ Cdl<\frac{P}{4G}<0\ for\ G<0\ \ (impossible) \end{cases}$$

- $\frac{A-\sqrt{A^2+B}}{2S(4\,Cdl\,G-P)}<\theta \quad \Rightarrow \quad A-\sqrt{A^2+B}<2S\theta\,(4\,Cdl\,G-P)$, which is always true
$$\Rightarrow \quad -(4\,Cdl\,G-P)\,(S\theta+1)-\sqrt{A^2+B}<0$$
(with some conditions on Cdl and G to obtain $\sqrt{A^2+B}>0$).
- $\frac{\theta}{2}<\frac{A-\sqrt{A^2+B}}{2S(4\,Cdl\,G-P)} \quad \Rightarrow \quad S\theta\,(4\,Cdl\,G-P)<A-\sqrt{A^2+B}$, that is impossible.
$$\Rightarrow \quad 0<-(4\,Cdl\,G-P)-\sqrt{A^2+B}$$

These results invalidate this hypothesis.

Hypothesis 2. $(4\ Cdl\ G-P)<0$

$$(4\,Cdl\,G-P)\ <0$$
$$\Rightarrow \quad \begin{cases} 0<Cdl<\frac{P}{4G}\ for\ G>0 \\ Cdl>0>\frac{P}{4G}\ for\ G<0\ \ (always\ true) \end{cases}$$

$$\frac{A-\sqrt{A^2+B}}{2S(4\,Cdl\,G-P)}<\theta$$
$$\Rightarrow \quad A-\sqrt{A^2+B}>2S(4\,Cdl\,G-P)$$

$$\Rightarrow \quad ((4\,Cdl\,G-P)\,(S\theta-1)-2S(4\,Cdl\,G-P))-\sqrt{A^2+B}>0$$
$$\Rightarrow \quad (A-C)-\sqrt{(A-C)^2+\left(B+2AC-C^2\right)}>0 \quad with\ C=2S(4\,Cdl\,G-P)$$
$$\Rightarrow \quad B+2AC-C^2<0$$

$$\Rightarrow \quad -4S\theta(4\cdot Cdl\cdot G-P)^2+2\cdot S\cdot\theta\,(4\cdot Cdl\cdot G-P)\cdot(4\cdot Cdl\cdot(G-S)-$$
$$\Rightarrow \quad 4\cdot Cdl\cdot(G+S)-P<0 \quad \Rightarrow \quad \begin{cases} 0<Cdl<\frac{P}{4(G+S)}\ for\ (G+S)>0 \\ Cdl>0>\frac{P}{4(G+S)}\ for\ (G+S)<0\ \ (alwa \end{cases}$$

$$\frac{\theta}{2}<\frac{A-\sqrt{A^2+B}}{2S(4\,Cdl\,G-P)} \quad \Rightarrow \quad S\theta\,(4\,Cdl\,G-P)>A-\sqrt{A^2+B}$$
$$\Rightarrow \quad \sqrt{A^2+B}>-(4\,Cdl\,G-P)>0$$

$$\Rightarrow \quad (4\,Cdl\,G-P)^2<A^2+B$$
$$\Rightarrow \quad Cdl>0>\frac{P}{4}\frac{\theta}{G\theta-2} \quad (always\ true)$$

As a result, for $S>0$, required conditions are $\begin{cases} Cdl<\frac{P}{4(G+S)}\ for\ (G+S)>0 \\ Cdl>0\ for\ (G+S)<0 \end{cases}$.

C.3. All cases

To summarize all cases

$S<0 \Rightarrow 0<\theta_{OONf=\infty}<\theta_{OONf}<\theta_{OONf=0}=\frac{\theta}{2}$	
$G-S>0$	$G-S<0$
$0<Cdl<\frac{P}{4(G-S)}$	$0<Cdl$
$S>0 \Rightarrow \theta>\theta_{OONf=\infty}>\theta_{OONf}>\theta_{OONf=0}=\frac{\theta}{2}$	
$G+S>0$	$G+S<0$
$0<Cdl<\frac{P}{4(G+S)}$	$0<Cdl$
Generalization $\forall S$	
$G+\lvert S\rvert>0$	$G+\lvert S\rvert<0$
$0<Cdl<\frac{P}{4\left(G+\lvert S\rvert\right)}$	$0<Cdl$

References

[1] R.G. Nuzzo, D.L. Allara, Adsorption of bifunctional organic disulfides on gold surfaces, J. Am. Chem. Soc. 105 (1983) 4481–4483, https://doi.org/10.1021/ja00351a063.

[2] J.C. Love, L.A. Estroff, J.K. Kriebel, R.G. Nuzzo, G.M. Whitesides, Self-assembled monolayers of thiolates on metals as a form of nanotechnology, Chem. Rev. 105 (2005) 1103–1170, https://doi.org/10.1021/cr0300789.

[3] A.L. Eckermann, D.J. Feld, J.A. Shaw, T.J. Meade, Electrochemistry of redox-active self-assembled monolayers, Coord. Chem. Rev. 254 (2010) 1769–1802, https://doi.org/10.1016/j.ccr.2009.12.023.
[4] Bard, Electrochemical Methods: Fundamentals and Applications - Google Scholar, in: https://scholar.google.com/scholar_lookup?title=Electrochemical%20methods%3A%20fundamentals%20and%20applications&author=A.J.%20Bard&publication_year=2000, 2020, (accessed February 12, 2020).
[5] E. Laviron, Adsorption, autoinhibition and autocatalysis in polarography and in linear potential sweep voltammetry, J. Electroanal. Chem. Interfacial Electrochem. 52 (1974) 355–393, https://doi.org/10.1016/S0022-0728(74)80448-1.
[6] T.M. Nahir, E.F. Bowden, The distribution of standard rate constants for electron transfer between thiol-modified gold electrodes and adsorbed cytochrome c, J. Electroanal. Chem. 410 (1996) 9–13, https://doi.org/10.1016/0022-0728(96)04551-2.
[7] J. Gonzalez, J.-A. Sequí, Square wave voltcoulommetry analysis of the influence of the electrostatic environment on the electrochemical functionality of redox monolayers, ChemElectroChem 6 (2019) 2290–2301, https://doi.org/10.1002/celc.201900352.
[8] M.S. Ravenscroft, H.O. Finklea, Kinetics of electron transfer to attached redox centers on gold electrodes in nonaqueous electrolytes, J. Phys. Chem. 98 (1994) 3843–3850, https://doi.org/10.1021/j100065a047.
[9] J. Gonzalez, J.-A. Sequí, Kinetic implications of the presence of intermolecular interactions in the response of binary self-assembled electroactive monolayers, ACS Omega 3 (2018) 1276–1292, https://doi.org/10.1021/acsomega.7b01995.
[10] S.E. Creager, T.T. Wooster, A new way of using ac voltammetry to study redox kinetics in electroactive monolayers, Anal. Chem. 70 (1998) 4257–4263, https://doi.org/10.1021/ac980482l.
[11] E. Laviron, A.C. polarography and faradaic impedance of strongly adsorbed electroactive species: Part I. Theoretical and experimental study of a quasi-reversible reaction in the case of a Langmuir isotherm, J. Electroanal. Chem. Interfacial Electrochem. 97 (1979) 135–149, https://doi.org/10.1016/S0022-0728(79)80057-1.
[12] E. Laviron, A.C. polarography and faradaic impedance of strongly adsorbed electroactive species: Part II. Theoretical study of a quasi-reversible reaction in the case of a Frumkin isotherm, J. Electroanal. Chem. Interfacial Electrochem. 105 (1979) 25–34, https://doi.org/10.1016/S0022-0728(79)80336-8.
[13] S. Guo, J. Zhang, D.M. Elton, A.M. Bond, Fourier transform large-amplitude alternating current cyclic voltammetry of surface-bound azurin, Anal. Chem. 76 (2004) 166–177, https://doi.org/10.1021/ac034901c.
[14] A.M. Bond, N.W. Duffy, S.-X. Guo, J. Zhang, D. Elton, Changing the look of voltammetry, Anal. Chem. 77 (2005) 186 A–195 A, https://doi.org/10.1021/ac053370k.
[15] C.G. Bell, C.A. Anastassiou, D. O'Hare, K.H. Parker, J.H. Siggers, Theoretical treatment of high-frequency, large-amplitude ac voltammetry applied to ideal surface-confined redox systems, Electrochim. Acta 64 (2012) 71–80, https://doi.org/10.1016/j.electacta.2011.12.088.
[16] M.J. Honeychurch, G.A. Rechnitz, Voltammetry of adsorbed molecules. Part 1: reversible redox systems, Electroanalysis 10 (1998) 285–293, https://doi.org/10.1002/(SICI)1521-4109(199804)10:5<285::AID-ELAN285>3.0.CO;2-B.
[17] M.J. Honeychurch, G.A. Rechnitz, Voltammetry of adsorbed molecules. Part 2: irreversible redox systems, Electroanalysis 10 (1998) 453–457, https://doi.org/10.1002/(SICI)1521-4109(199806)10:7<453::AID-ELAN453>3.0.CO;2-F.
[18] E. Laviron, L. Roullier, General expression of the linear potential sweep voltammogram for a surface redox reaction with interactions between the adsorbed molecules: applications to modified electrodes, J. Electroanal. Chem. Interfacial Electrochem. 115 (1980) 65–74, https://doi.org/10.1016/S0022-0728(80)80496-7.
[19] E. Laviron, Surface linear potential sweep voltammetry: equation of the peaks for a reversible reaction when interactions between the adsorbed molecules are taken into account, J. Electroanal. Chem. Interfacial Electrochem. 52 (1974) 395–402, https://doi.org/10.1016/S0022-0728(74)80449-3.
[20] O. Aleveque, P.Y. Blanchard, C. Gautier, M. Dias, T. Breton, E. Levillain, Electroactive self-assembled monolayers: Laviron's interaction model extended to non-random distribution of redox centers, Electrochem. Commun. 12 (2010) 1462–1466, https://doi.org/10.1016/j.elecom.2010.07.039.
[21] O. Aleveque, E. Levillain, Electroactive mixed self-assembled monolayers: lateral interactions model updated to interactions between redox and non-redox species, Electrochem. Commun. 34 (2013) 165–169, https://doi.org/10.1016/j.elecom.2013.06.009.
[22] O. Aleveque, C. Gautier, M. Dias, T. Breton, E. Levillain, Phase segregation on electroactive self-assembled monolayers: a numerical approach for describing lateral interactions between redox centers, Phys. Chem. Chem. Phys. 12 (2010) 12584–12590, https://doi.org/10.1039/c0cp00085j.
[23] E. Laviron, General expression of the linear potential sweep voltammogram in the case of diffusionless electrochemical systems, J. Electroanal. Chem. Interfacial Electrochem. 101 (1979) 19–28, https://doi.org/10.1016/S0022-0728(79)80075-3.
[24] M.J. Honeychurch, A.M. Bond, Numerical simulation of Fourier transform alternating current linear sweep voltammetry of surface bound molecules, J. Electroanal. Chem. 529 (2002) 3–11, https://doi.org/10.1016/S0022-0728(02)00907-5.
[25] E. Laviron, A.C. Polarography and faradaic impedance of strongly adsorbed electroactive species: Part III. Theoretical complex plane analysis for a surface redox reaction, J. Electroanal. Chem. Interfacial Electrochem. 105 (1979) 35–42, https://doi.org/10.1016/S0022-0728(79)80337-X.
[26] C. Lambert, V. Kriegisch, A. Terfort, B. Zeysing, Heterogeneous electron transfer processes in triarylamine- and ferrocene-based self-assembled monolayers, J. Electroanal. Chem. 590 (2006) 32–36, https://doi.org/10.1016/j.jelechem.2006.02.017.
[27] D. González-Flores, M.L. Montero, An advanced experiment for studying electron transfer and charge storage on surfaces modified with metallic complexes, J. Chem. Educ. 90 (2013) 1077–1081, https://doi.org/10.1021/ed3004885.
[28] O. Aleveque, F. Seladji, C. Gautier, M. Dias, T. Breton, E. Levillain, Nitroxyl radical self-assembled monolayers on gold: versatile electroactive centers in aqueous and organic media, Chemphyschem 10 (2009) 2401–2404, https://doi.org/10.1002/cphc.200900448.
[29] V.D. Ivanov, Adsorption voltammetric peak: approximate calculation algorithm taking into account lateral interactions, J. Solid State Electrochem. 23 (2019) 1371–1377, https://doi.org/10.1007/s10008-019-04235-3.